Supporting Information

Novel two-dimensional ferromagnetic materials CrX_2 (X = O, S, Se) with high Curie temperature

Gang Xiao [a], Wen-Zhi Xiao [a]*, Qiao Chen [a], Ling-ling Wang [b]

[a] School of Computational Science and Electronics, Hunan Institute of Engineering, Xiangtan 411104,China

[b] School of Physics and Electronics, Hunan University, Changsha 410082, China

The search process of the evolutionary algorithm:

The global minimum energy configuration for CrO_2, CrS_2, and $CrSe_2$ binary compounds containing 3-12 atoms in each unit cell and a 1:2 element ratio is obtained by employing the evolutionary algorithm (EA) within USPEX (Universal Structure Predictor: Evolutionary Xtallography) software. In the iteration of the population, the initial population size is set to 90, the population size of each subsequent generation is 40, the population generation is 40 generations, and retain the first 50% of the energy of the current generation to generate offspring. During evolution, 50% of the population is generated by inheritance, 30% is generated randomly by space group symmetry, 10% is generated by lattice mutation, and 10% is generated by soft mode mutation. A simulation is discontinued early when the optimal structure remains unchanged for 20 generations.

*Corresponding author: xiaowenzhi@hnie.edu.cn

Figure S1

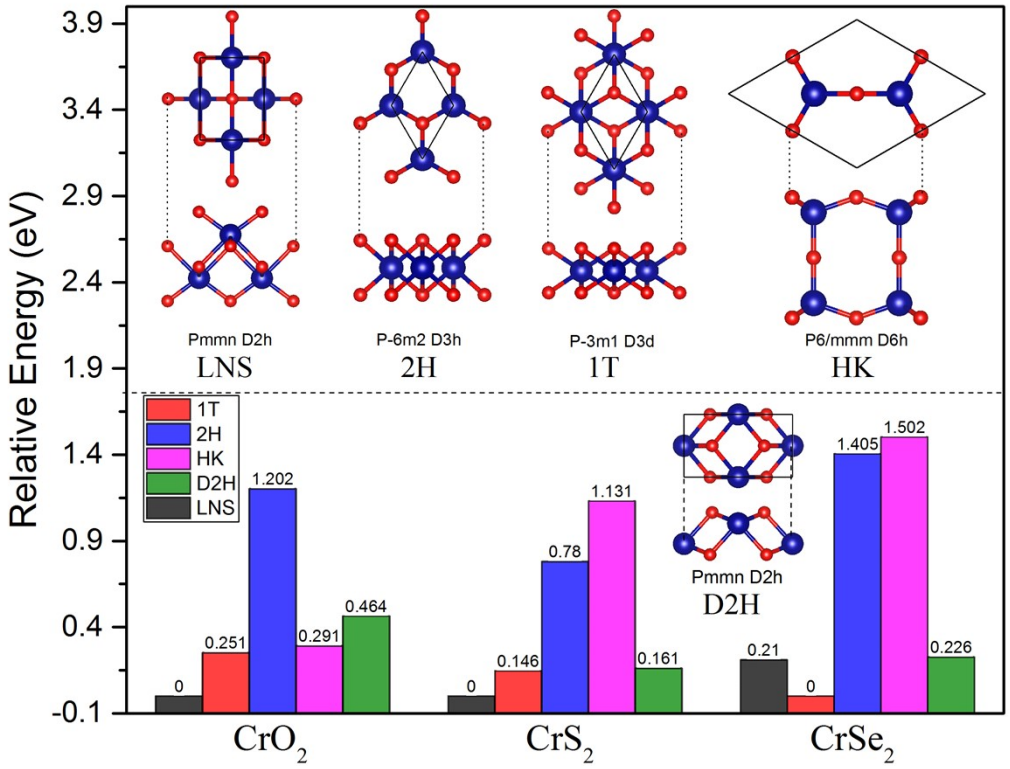

Figure S1. Calculated relative energies (eV per chemical formula) which refer to that of the most stable 2D CrX_2 (X = O, S, Se) structure. Inset shows the corresponding top and side views of various configurations. The CrO_2 and CrS_2 monolayers with lepidocrocite-type structure (LNS) are most stable in energy, while the $CrSe_2$ with 1T structure is most stable.

Table S1. Optimized structural properties of the four different 2D CrO_2 crystal structures. ***a***, ***b*** and ***c*** are the lattice constants. Atomic positions are the group Wyckoff positions for each independent atoms in fractional coordinates. All the parameters are calculated by GGA+U method.

Structure	LNS	1H	1T	HK	D2H
Space group	Pmmn (#59)	P-6m2 (#187)	P-3m1 (#164)	P6/mmm (#191)	Pmmn (#59)
a (Å)	2.935	2.626	2.900	5.810	2.906
b (Å)	3.779	2.626	2.900	2.900	5.013
c (Å)	25.0	25.0	25.0	25.0	25.0
Positions	O(0.5,0.5,0.416)	O(2/3,1/3,0.453)	O(2/3,1/3,0.461)	O(1/3,2/3,0.5)	O(0.0,0.76,0.461)
	O(0.5,0.5,0.519)	Cr(0.0,0.0,0.5)	Cr(0.0,0.0,0.5)	O(0.5,0.5,0.595)	Cr(0.0,0.5,0.519)
	Cr(0.0,0.5,0.459)			Cr(1/3,2/3,0.571)	

Figure S2

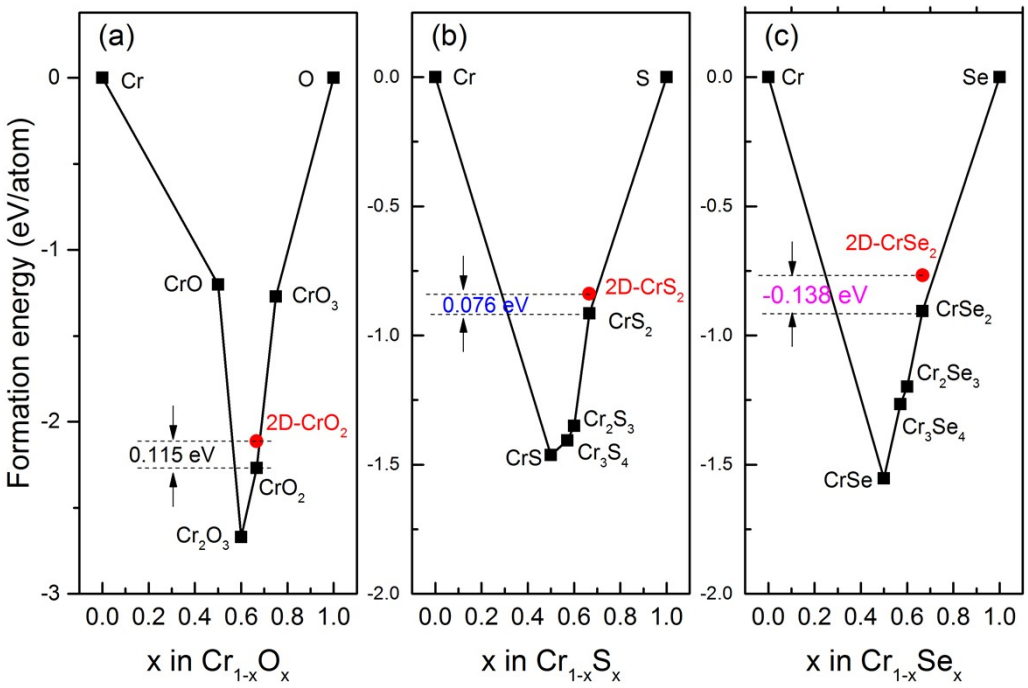

Figure S2. Calculated formation energy convex hull for Cr-X systems. The red markers indicate the formation energies of 2D materials with lepidocrocite-type (LNS) structure. The elemental reference states are taken from bulk Cr, and molecular O_2, S_8, and Se_8, as motioned in the main text. The stable intermediate phases of Cr-X systems are selected from the databases of Materials Project [1] (https://materialsproject.org/materials), Inorganic Crystal Structure Database (ICSD) [2], and the references [3, 4, 5]. Van der Waals correction was considered at the vdW-DF level [6], with the optB86b functional for the exchange potential [7].

Table S2. Calculated charge transfer for inner and surface X atoms sites (X_{in} and X_{surf}) and Cr of CrX_2 monolayers based on Bader analysis [8] at PBE+U level. Subscript in and surf denote the inner and surface X atoms.

System	X_{in} (electron)	X_{surf} (electron)	Cr (electron)
CrO_2	+ 0.8148	+ 1.1125	- 1.9274
CrS_2	+ 0.5071	+ 0.7787	-1.2858
$CrSe_2$	+ 0.4275	+ 0.6484	-1.0758

Table S3. Calculated values of exchange coupling parameters J_i and local magnetic moment on Cr site for electron and hole doped CrO_2 monolayer at HSE06 leve. The doped concentrations of electron and hole are 0.1 *e* and 0.2 *e* per Cr atom, respectively.

System	J_1 (meV)	J_2 (meV)	J_3 (meV)	M_{Cr} (μ_B)
CrO_2 + electron	55.5	0.88	6.97	2.541
CrO_2 + hole	70.15	3.32	1.91	2.540

Figure S3

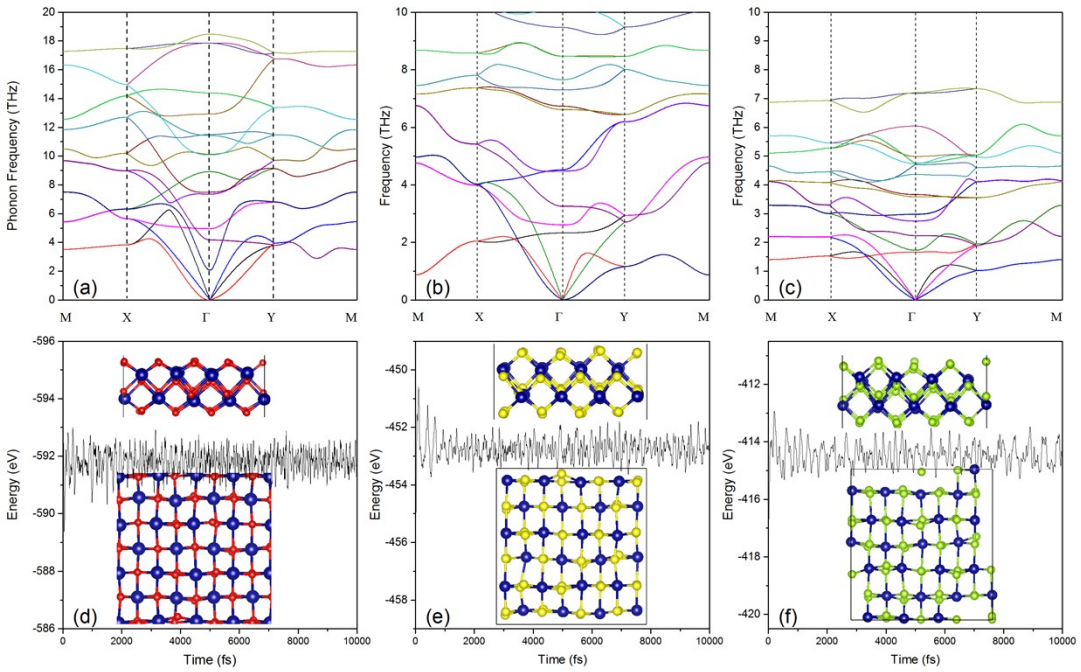

Figure S3. Phonon band diagrams of the (a) CrO_2, (b) CrS_2, and (c) $CrSe_2$ monolayers with lepidocrocite-type structure (LNS). Potential energy as function of time for (d) CrO_2, (e) CrS_2, and (d) $CrSe_2$ monolayers *ab* initio molecular dynamics simulations at 500 K. Inset shows the corresponding snapshots CrX_2 structures at the end of 10 ps.

Figure S4

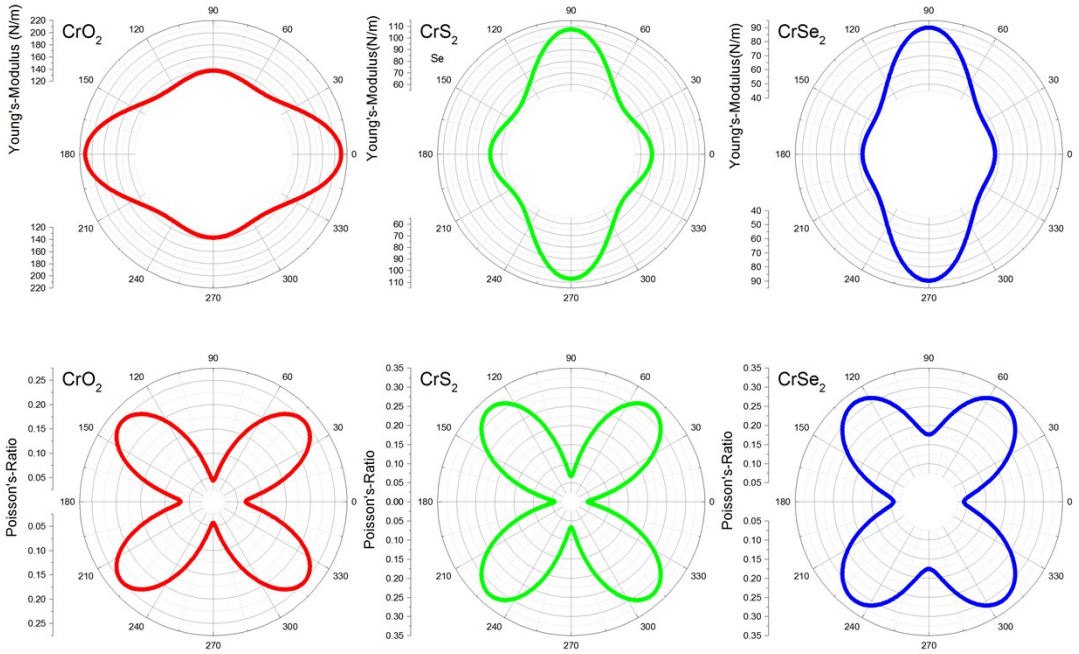

Figure S4. Calculated orientation-dependent Young's modulus Y(θ) and Poisson's ratio $v(\theta)$. The angle θ measured clockwise from the referent x-axis. We calculated the orientation-dependent Poisson's ratio v and Young's modulus Y by using the following equations:

$$\begin{cases} Y(\theta) = \dfrac{Y_{zz}}{\cos^4\theta + d_2 \sin^2\theta\cos^2\theta + d_3 \sin^4\theta} \\ v(\theta) = \dfrac{v_{zz}\cos^4\theta - d_1 \sin^2\theta\cos^2\theta + v_{zz}\sin^4\theta}{\cos^4\theta + d_2 \sin^2\theta\cos^2\theta + d_3 \sin^4\theta} \end{cases} \tag{5}$$

where d_1, d_2, d_3, Y_{zz}, and v_{zz} are elasticity-constant-related variables described in detail in the references[9, 10, 11].

Figure S5

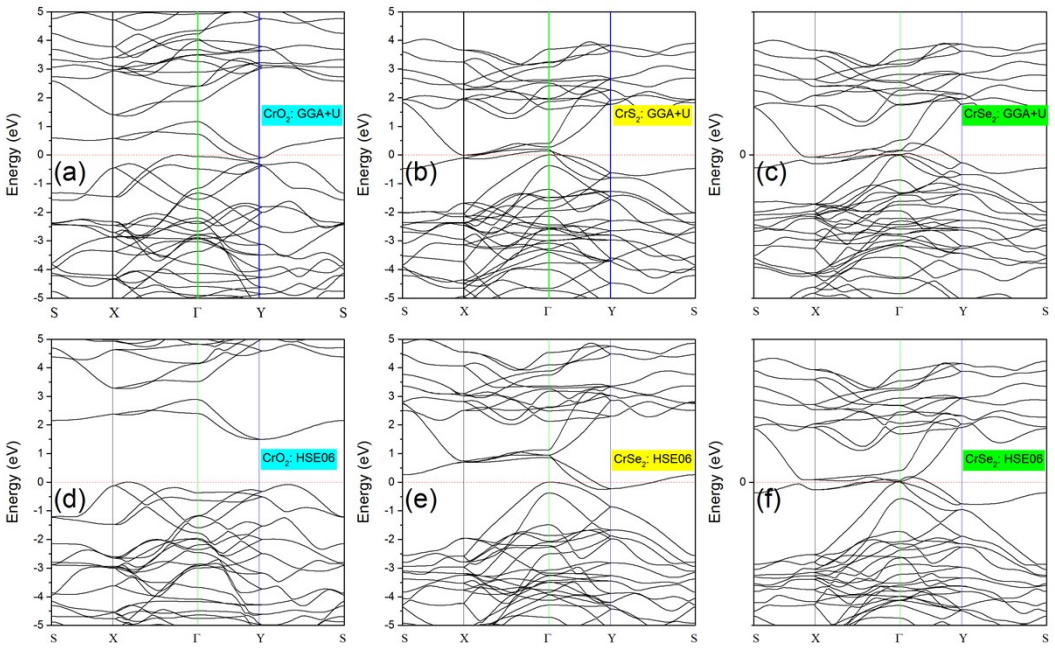

Figure S5. Electronic band structures of the (a) CrO_2, (b) CrS_2, (c) $CrSe_2$ monolayers at GGA+U+SOC level, and (d) CrO_2, (e) CrS_2, (f) $CrSe_2$ monolayers at HSE06+SOC level. The Fermi level is denoted by a dashed line at 0.0 eV. The electronic band structures do not appreciably change with respect to those obtained from GGA+U and HSE06 without SOC.

Figure S6.

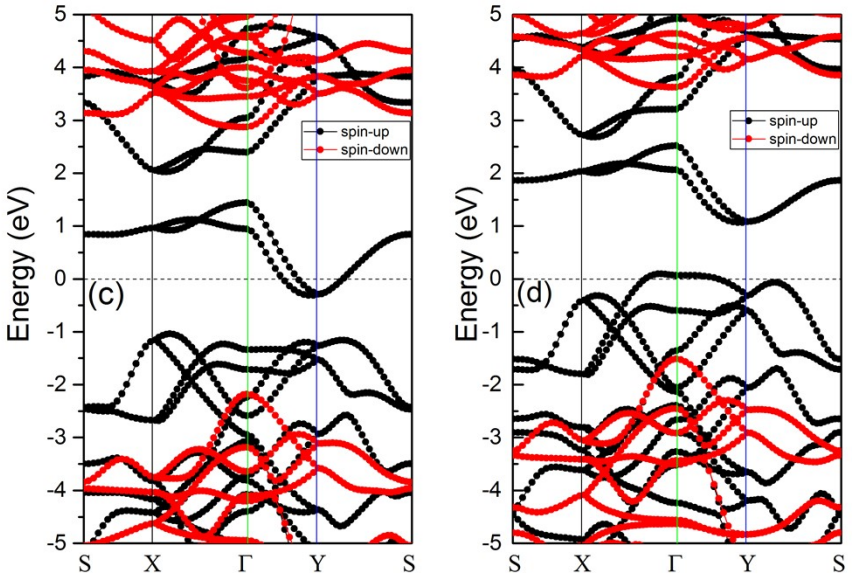

Figure S6. Electronic band structures of (a) electron- and (b) hole-doped CrO_2 monolayers at HSE06 level. The doped concentrations of electron and hole are 0.1 *e* and 0.2 *e* per Cr atom, respectively.

Figure S7.

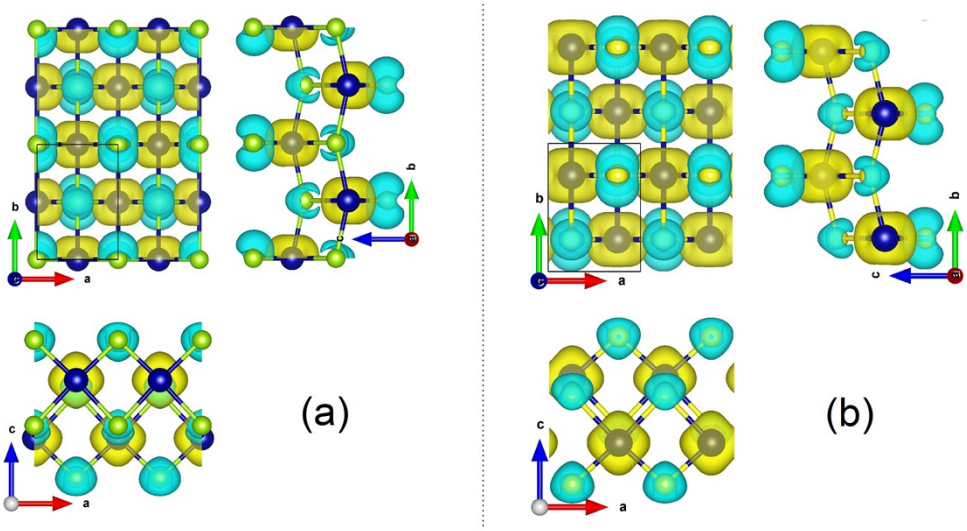

Figure S7. Spin charge densities distribution with an isovalue of 0.01 e/ Å^3 for (a) CrS_2 and (b) $CrSe_2$ monolayers. The contour profile with yellow and green indicates spin-up and spin-down polarization

Figure S8.

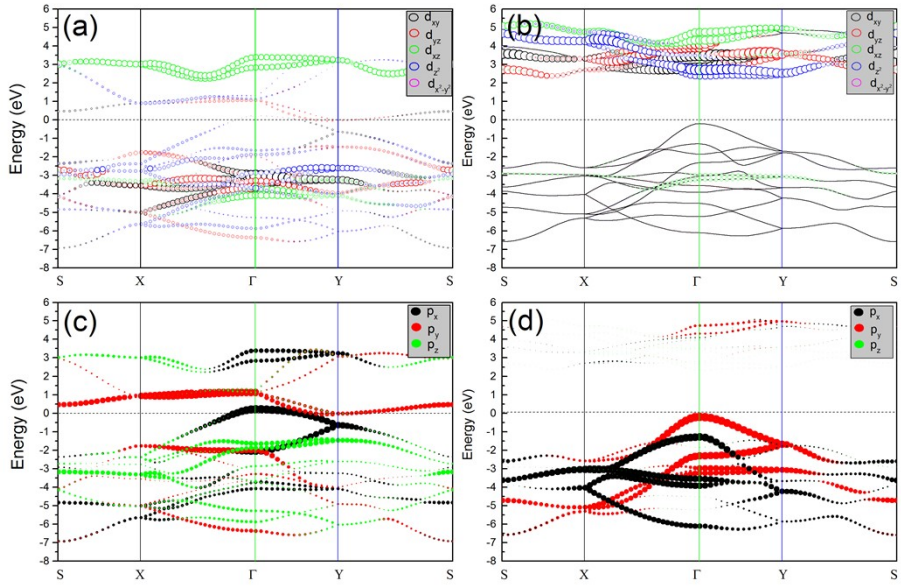

Figure S8. Orbital projected band structures on Cr:3*d* orbitals in (a) spin-up and (b) spin-down channels, on S:3*p* orbitals in (c) spin-up and (d) spin-down channels for CrS_2 monolayer.

Figure S9.

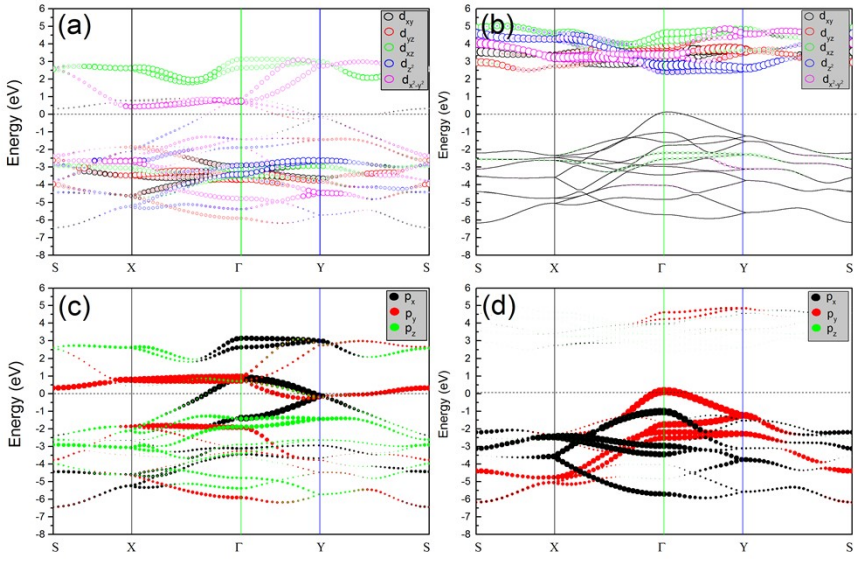

Figure S9. Orbital projected band structures on Cr:3*d* orbitals in (a) spin-up and (b) spin-down channels, on Se:4*p* orbitals in (c) spin-up and (d) spin-down channels for $CrSe_2$ monolayer.

Figure S10.

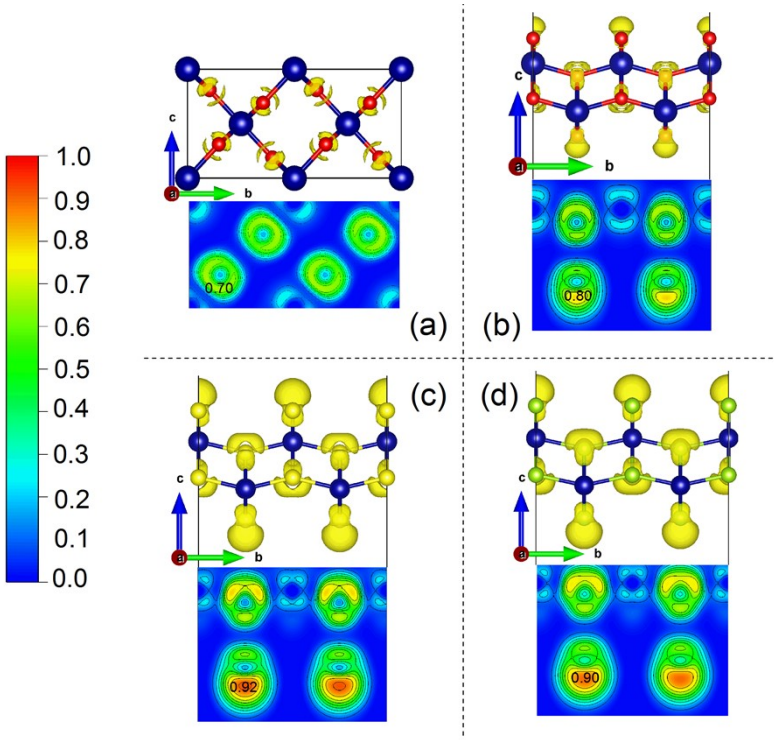

Figure S10. Electron localization functions of (a) bulk CrO_2 in rutile phase, monolayer (b) CrO_2, (c) CrS_2, and (d) $CrSe_2$ at the PBE level of theory. The plots of charge density difference characterize similar conclusion that the surface X atoms carry much more charge than that of the inner X atom for CrX_2 monolayers.

---

[1] A. Jain, S. P. Ong, G. Hautier, W. Chen, W. D. Richards, S. Dacek, S. Cholia, D. Gunter, D. Skinner, G. Ceder, K. A. Persson, Commentary: the Materials Project: a materials genome approach to accelerating materials innovation. *APL Mater.* 2013, **1 (1)**, 011002.

[2] A. Belsky, M. Hellenbrandt, V. L. Karen, P. Luksch, New developments in the Inorganic Crystal Structure Database (ICSD): accessibility in support of materials research and design. *Acta Crystallogr., Sect. B: Struct. Sci.* 2002, 58, 364−369.

[3] G. K. Rajendran Nair, A. Abdelaziem, X. Zhao, X. Wang, D. Hu, Y. Wu, ... & Z. Liu, Chemical Vapor Deposition of Phase Pure 2D 1T−CrS_2. *Phys. Status Solidi RRL*, 2022, **16**, 2100495.

[4] H. Xiao, W. Zhuang, L. Loh, T. Liang, A. Gayen, P. Ye, ... & M. Xu,Van der Waals Epitaxial Growth of 2D Layered Room−Temperature Ferromagnetic CrS_2. *Adv. Mater. Interfaces*, 2022, 2201353.

[5] B. Li, Z. Wan, C. Wang, P. Chen, B. Huang, X. Cheng, ... & X. Duan, Van der Waals epitaxial growth of air-stable $CrSe_2$ nanosheets with thickness-tunable magnetic order. *Nat. Mater.*, 2021, **20**, 818-825.

[6] Dion, M., Rydberg, H., Schröder, E., Langreth, D. C. & Lundqvist, B. I. Van der Waals density functional for general geometries. *Phys. Rev. Lett.* 2004, **92**, 246401.

[7] J. Klimeš, D. R. Bowler, A. Michaelides, Van der Waals density functionals applied to solids. *Phys. Rev. B*, 2011, **83**, 195131.

[8] E. Sanville, S. D. Kenny, R. Smith, G. Henkelman, Improved Grid-Based Algorithm for Bader Charge Allocation. J. Comput. Chem. 2007, 28, 899−908.

[9] L. Wang, A. Kutana, X. Zou and B. I. Yakobson, Electro-mechanical anisotropy of phosphorene. *Nanoscale*, 2015, **7**, 9746–9751.

[10] H. Wang, X. Li, P. Li, J. Yang, δ-Phosphorene: a two dimensional material with a highly negative Poisson's ratio. *Nanoscale*, 2017, **9**(2), 850-855.

[11] E. Cadelano, P. L. Palla, S. Giordano, L. Colombo, Elastic properties of hydrogenated grapheme. *Phys. Rev. B*, 2010, 82(23), 235414.